NIH Public Access
Author Manuscript
Vision Res. Author manuscript; available in PMC 2012 October 1.

Published in final edited form as:
Vision Res. 2011 October 1; 51(19): 2132–2138. doi:10.1016/j.visres.2011.08.008.

The relationship between peripapillary crescent and axial length: implications for differential eye growth

Toco YP Chui[*], **Zhangyi Zhong**, and **Stephen A Burns**
School of Optometry, Indiana University, 800 E. Atwater Ave, Bloomington, IN, 47405, USA

Abstract

We evaluated the relationship between the size of the peripapillary crescent and the axial length (AL) of the eye as well as the fine structure of the peripapillary crescent in selected eyes. Infrared fundus imaging and spectral domain optical coherence tomography (SDOCT) (Spectralis HRA +OCT, Heidelberg Engineering, Germany) centered at the fovea were performed on 72 healthy adults. On the infrared fundus images, we measured (a) the distance between the foveola and the temporal edge of the optic disc (FOD) and (b) the distance between the foveola and the temporal edge of the peripapillary crescent (FOC) (if present). A peripapillary crescent presented at the nasal margin of the disc in 64% of the subjects. The FOD and FOC were 4.22mm±0.46 and 3.97mm±0.25, respectively. Only the FOD was significantly correlated with axial length. As AL increased by 10%, the FOD increased by 13%, the outer neural retina only expanded by 4% (as indicated by the FOC). This result emphasizes that retinal stretching may not mirror scleral growth, and the existence in some eyes of a difference between the photoreceptor margin and RPE margin suggests that within the retina there could be slippage during eye growth.

Keywords

myopia; optic disc; optic disc crescent; spectral domain optical coherence tomography; adaptive optics scanning laser ophthalmoscope

1. Introduction

The most visible change in the appearance of the myopic fundus is the presence of the peripapillary crescent, which is also known as β-peripapillary atrophy (Curcio, Saunders, Younger & Malek, 2000; Jonas, Nguyen, Gusek & Naumann, 1989; Kubota, Jonas & Naumann, 1993). The bright appearance of the crescent reflects the absence of the retinal pigment epithelium (RPE) and choroid. The presence of an optic disc crescent therefore suggests that the excessive scleral stretching as myopia develops is not mirrored by the RPE and choroid at the region of the crescent.

The structural changes due to the formation of the peripapillary crescent have been studied thoroughly with histological samples. Histological findings have shown that the photoreceptors, RPE, and choroid fall short at the temporal margin of the crescent in myopia (Grossniklaus & Green, 1992) with a partial loss of the photoreceptors and a complete loss of the RPE at the atrophic area (Curcio et al., 2000; Kubota et al., 1993). The sclera underneath the crescent also appears stretched in pathological myopia (Yasuzumi, Ohno-Matsui, Yoshida, Kojima, Shimada, Futagami, Tokoro & Mochizuki, 2003).

[*]Corresponding author: ypchui@indiana.edu Contact no: 1-812-855-9884.

NIH-PA Author Manuscript
NIH-PA Author Manuscript
NIH-PA Author Manuscript

NIH-PA Author Manuscript

NIH-PA Author Manuscript

NIH-PA Author Manuscript

Clinically, it has been shown that the frequency of peripapillary crescents increases with increasing axial length (Curtin & Karlin, 1971; Hendicott & Lam, 1991) from 0% in eyes with AL of 20.0–21.4mm to 100% in eyes with AL of 28.5mm (Curtin & Karlin, 1971). Although the presence of a crescent is associated with growth of the eye, a previous longitudinal study has shown that the distance between the foveola and the temporal edge of the crescent remains constant as myopia progresses (Nakazawa, Kurotaki & Ruike, 2008). All these findings suggest that the crescent represents an area where the strain resulting from scleral stretching, is accompanied by a slippage of the major retinal/choroidal layers as myopia progresses. This is also supported by the increase in photoreceptor spacing on all retinal meridians with increasing eye length, except along the nasal retinal meridian (Chui, Song & Burns, 2008b), presumably due to a separation of the retina from the disc during myopic eye growth.

In the present study, we evaluate the relationship between the peripapillary crescent and axial length in 72 healthy eyes using different imaging techniques. We tested the hypothesis that retinal and choroidal layer slippage is associated with myopic eye growth as reflected in adult eye length measurements.

2. Methods

2.1 Subjects

Seventy-two healthy subjects (35 males and 37 female; age range 20–67 years, mean = 38, SD=±14) participated in this study. All subjects received a complete eye examination, including a subjective refraction and fundus examination. Exclusion criteria for this study included any evidence of retinal pathology (other than myopia) or systemic diseases. Spherical equivalent refractive errors ranged from +2.00D to −13.75D (mean −2.73D; SD = ±3.21) with astigmatism less than −2.00D when referenced to the spectacle plane. All subjects had best corrected visual acuity of 20/20 or better. Only the right eye of each subject was tested in this study. Informed consent was obtained after a full explanation of the procedures and consequences of the study. This study protocol was approved by the Indiana University Institutional Review Board and complied with the requirements of the Declaration of Helsinki.

2.2 Procedures

Axial length measurement—Five axial length (AL) measurements of each eye were made using an IOL Master (Carl Zeiss Meditec, Dublin, California), and we reported the mean AL for each eye.

Infrared fundus imaging and spectral domain optical coherence tomography (SDOCT) imaging—Infrared fundus imaging and SDOCT imaging were performed to obtain both *en face* fundus images and cross-sectional measurements of the posterior pole (Spectralis HRA + OCT, Heidelberg Engineering, Heidelberg, Germany). In this experiment, an infrared fundus image covering 30° of the central retina was obtained for each eye, from which we measured the distance between (1) the foveola and temporal edge of the optic disc (**FOD**) and (2) the foveola and temporal edge of the peripapillary crescent (**FOC**) (if present) (Figure 1) along the horizontal axis. The retinal magnification differences induced by different axial lengths were factored into a calculation of linear retinal units as described by a previous study (Bennett, Rudnicka & Edgar, 1994).

The foveola was located using SDOCT images obtained using a super luminescent diode with a wavelength of 870nm as a light source. The axial and lateral resolutions of the SDOCT were approximately 7μm and 14μm, respectively. A 15° × 15° raster scan centered

NIH-PA Author Manuscript

NIH-PA Author Manuscript

NIH-PA Author Manuscript

at the fovea consisting of 73 horizontal b-scans was obtained in each subject using the manufacturer supplied eye-tracking feature (Automatic Real Time, ART). Each b-scan was composed of 768 equally spaced a-scans. The separation between b-scans was 60μm. To reduce speckle noise, each b-scan was created by averaging 20 frames. The foveola on the infrared fundus image was defined as the corresponding location of minimum retinal thickness on the SDOCT b-scan in each subject. All fundus images and b-scan images were exported as tiff files for further image processing.

High resolution imaging of the optic disc crescent—SDOCT and adaptive optics scanning laser ophthalmoscope (AOSLO) imaging were performed on the optic disc crescent in 6 of the eyes (1 emmetrope and 5 myopes). SDOCT imaging was performed to obtain cross-sectional measurement of the optic disc and optic disc crescent. In addition to the horizontal b-scan centered at the fovea, a 20° × 15° raster scan centered at the optic disc was performed in 6 subjects. Each b-scan was composed of 1,024 equally spaced a-scans. The separation between b-scans was ~120μm. Each b-scan was created by averaging 20 consecutive frames.

The integrity of RNFL and cone photoreceptors at the optic disc crescent was investigated using the Indiana AOSLO (Ferguson, Zhong, Hammer, Mujat, Patel, Deng, Zou & Burns, 2010). The Indiana AOSLO system is composed of three primary optical subsystems of importance to the current study, the wavefront sensor and dual deformable mirror subsystem, the confocal imaging subsystem, and the wide field imaging subsystem. The light source for high resolution imaging was provided by a supercontinuum source (Fianium, Inc) with an 840nm filter (Burns, Zhong, Qi & Elsner, 2010). Wavefront errors were detected with a Shack Hartmann sensor operating at 18.5 Hz. The adaptive optics control of the system was maintained using two deformable mirrors sequentially (Mirao 52D - Imagine Eyes and BMC MultiDM – Boston Micromachines). We firstly activated the Mirao mirror to correct low order aberrations, and then the BMC mirror to correct high order aberrations. The imaging raster was provided by a 10 kHz horizontal scanning galvanometer and a programmable vertical scan galvanometer. For these experiments the vertical scan was programmed to provide full frame images of 2° × 1.8° at a frame rate of 18.5Hz. Light returning from the retina passes through a confocal aperture optically conjugate to the retinal plane. The confocal aperture was 200μm, approximately 7 times the airy disc radius. Our AOSLO system would provide lateral resolution of less than 2.5 microns for a diffraction limited emmetropic eye (Rayleigh Criterion, pupil size 6.8mm) and real performance approaches this for this pupil size and pinhole. Pupil dilation with 0.5% tropicamide was performed on 2 of the 6 subjects for AOSLO imaging. Other subject's pupils were sufficiently large to allow imaging of cones and RPE cells without dilation. Subject's head movements were stabilized using a chin and head rest. Image processing was performed offline as described in our previous studies (Chui, Song & Burns, 2008a; Chui et al., 2008b)

3. Results

Axial length ranged from 22.00mm to 27.88mm (mean 24.59mm; standard deviation ±1.34) and was linearly related to spherical equivalent (r^2=0.72; p<0.01).

3.1 Infrared fundus imaging and spectral domain optical coherence tomography imaging

Figure 2 shows the variation of the FOD and FOC with axial length. Both the FOD and FOC were statistically correlated with axial length with the Pearson correlation coefficient of 0.64 and 0.31, respectively (p-value <0.05). The mean and standard deviation of the FOD and FOC in all 72 subjects were 4.22±0.46 mm (range = 3.48–5.47mm) and 3.95±0.27 mm (range = 3.48–4.74mm), respectively. Note that the regression line of these 72 FOC

NIH-PA Author Manuscript

NIH-PA Author Manuscript

NIH-PA Author Manuscript

measurements included the data from the 26 subjects who did not have optic disc crescents (i.e. FOC = FOD). Optic disc crescents presented in 46 subjects (64% of the total subjects). When the subjects without optic disc crescent were excluded from the statistical analysis of FOC, the mean and standard deviation of the FOC was 3.97±0.25 mm (46 subjects; range = 3.59–4.67mm) with the Pearson correlation coefficient of 0.24 (p-value=0.1). Figure 3 shows the horizontal width of the optic disc crescent (the difference of FOD and FOC) as a function of axial length in subjects with optic disc crescent. The mean and standard deviation of the horizontal width of the optic disc crescent was 0.42±0.35 mm (range = 0.09–1.34mm) with the Pearson correlation coefficient of 0.57 (p-value<0.01); Crescents were present in all eyes with axial length greater than 26.08mm.

3.2 High resolution imaging of the optic disc crescent

SDOCT and AOSLO imaging were performed on the optic disc crescent in 6 of the eyes (1 emmetrope and 5 myopes). Details of the subject demographics are shown in Table 1.

SDOCT images—In all 6 tested subjects, SDOCT showed no retinal nerve fiber layer (RNFL) abnormality around the optic disc. In 5 subjects with an optic disc crescent, the inner nuclear layer (INL) and the inner plexiform layer (IPL) showed gradual thinning from the temporal edge of the crescent towards the temporal edge of the optic disc. In contrast, the INL and the IPL ended more abruptly on the nasal side of the optic disc. Figure 4b, 5b, and 6b show the SDOCT images across the crescent in subject 1, 3, and 5, respectively.

From the SDOCT image corresponding to the temporal crescent (crescent located on the temporal side of the optic disc), the external limiting membrane (ELM), the outer/inner segment junction (OS/IS), and the retinal pigment epithelium complex (RPE+) did not reach the temporal edge of the optic disc but ended gradually in the temporal edge of the crescent. In contrast, the ELM, OS/IS, and RPE+ were distinguishable all the way to the nasal edge of the optic disc. Disruptions of the ELM and OS/IS were observed on the SDOCT image corresponding to the temporal edge of the crescent. Atrophy of the RPE+ and ONL was also found within the crescent (Figure 5b & 6b).

In the subject without crescent, gradual thinning of the ONL and OPL towards the optic disc was observed on both temporal and nasal sides of the optic disc. The ELM, OS/IS, and RPE + ended closely to the edge of the optic disc. No obviously ELM and OS/IS disruption and RPE+ atrophy were found at the edge of the optic disc.

AOSLO images—Figure 4–6(c–e) show the high resolution AOSLO images of RNFL and cone photoreceptor layer at the temporal edge of the crescent in subject 1, 3, 5, and 4, respectively. AOSLO images within the crescent showed normal RNFL striation. The RNFL bundles were well organized and distinctive. No localized uneven reflectivity of the RNFL was observed. Cone photoreceptors were visualized at the temporal margin of the crescent, which agrees with SDOCT estimates of the position of the edge of the ONL. In figure 4–6 (d & e), cone photoreceptors are seen as bright spots due to their fiber optic waveguide properties (Burns, Wu, Delori & Elsner, 1995; Miller, Williams, Morris & Liang, 1996; Roorda & Williams, 2002; Stiles & Crawford, 1933; van Blokland, 1986). Rods are not readily seen with the smaller pupils used in this study. RPE cells near the crescent were visualized in 4 of the 6 subjects using directly back scattered light. Figure 7b & 7c show that several RPE cells were visualized at the retinal area just outside the crescent in subject 4. Hexagonal packing structure of the RPE cells is also observed. The center to center spacing of the RPE cells was ~15.2um.

NIH-PA Author Manuscript

NIH-PA Author Manuscript

NIH-PA Author Manuscript

4. Discussion

4.1 Retinal Dimensions

In the present study, we have investigated the relationship between peripapillary crescent and axial length in 72 eyes with different axial lengths using different retinal imaging techniques. Direct comparisons of the data from previous studies are difficult, owing to the differences in the definition of FOD and FOC. While previous studies measured the retinal distance along a line which connects the foveola to the optic disc and the temporal crescent margin directly, the present study measured the horizontal retinal distance between the foveola and the optic disc (Figure 1). Assuming that the foveola is located 6.11° below the horizontal meridian passing through the optic disc center (Williams & Wilkinson, 1992) and this angular distance is relatively constant among subjects (Rohrschneider, 2004) , we computed the retinal distance between the foveola and the optic disc margin along the horizontal axis (computed FOD) for the data obtained from previous studies (Mok & Lee, 2002; Williams & Wilkinson, 1992). Our FOD data is approximately 5–10% larger than the computed FOD data reported by previous studies for normal healthy subjects; our mean FOC data of 3.97mm, however, are in close agreement with the FOD data reported by the same studies with the mean value of 3.82mm (Mok & Lee, 2002) and 4.01mm (Williams & Wilkinson, 1992).

Our FOD and FOC data are consistent with a previous longitudinal study that while the FOD increases, the FOC remains constant as myopia progresses (Nakazawa et al., 2008). According to our findings, as axial length increased by 10%, the FOD increases by 13%, but the FOC only expands by 4%. The FOD and FOC data in both studies imply that the outer neural retina does not follow the retinal stretching pattern along the nasal side of the eye. That is, it emphasizes that stretching in the outer neural retina may not mirror that of the sclera and subretinal tissue. These results explains our previous finding of cone packing density between the fovea and optic nerve changed less than that predicted by observed eye growth (Chui et al., 2008b). It appears as though the retina beneath the papillomacular bundle is maintaining an approximately constant length, and the growth induced strain which would otherwise cause retinal stretching, is ameliorated in some cases by an increased crescent size.

If optic disc crescent formation is due to excessive ocular growth as myopia progresses, one might expect that the width of the crescent would associate with increasing myopia. Unlike the present study, a previous study has shown that the size of crescents was not associated with increasing AL after excluding the eyes without crescents (Fulk, Goss, Christensen, Cline & Herrin-Lawson, 1992; Hendicott & Lam, 1991). This discrepancy is probably due to the fact that our data of crescent width are measured after correcting the retinal magnification induced by different axial lengths.

Understanding the changes in retinal dimensions associated with eye growth could improve our ability to better understand the eye growth pattern during myopia development. Axial elongation in myopia necessarily implies an increase in ocular surface area, suggesting a mechanical stretching on the retinal layers. Strang and colleagues (1998) suggested three types of stretching models in myopia: global expansion, posterior pole stretching and equatorial stretching (Strang, Winn & Bradley, 1998). While the global stretching model assumes a uniform stretching across the eyeball, the posterior pole stretching model assumes that ocular stretching solely occurs at the posterior pole. Both the global stretching and posterior stretching model predict an increase in FOD and FOC due to the radial expansion pattern at the posterior pole. On the other hand, the equatorial stretching model assumes that ocular stretching is limited to the equator of the eye, and would therefore, predict a constant FOD and FOC due to the unaffected posterior pole. If the posterior pole expands uniformly

NIH-PA Author Manuscript

NIH-PA Author Manuscript

NIH-PA Author Manuscript

as in the global expansion model, we would expect that a 10% increases in axial length would induce a 10% in both FOD and FOC (Figure 8, **dashed lines**). In contrast, if the axial elongation is mainly due to the stretching at the equator as in the equatorial stretching model, we would expect a constant FOD and FOC (Figure 8, **light solid lines**). According to our data, however, the FOD and FOC increase approximately 13% and 4%, respectively. That is, while our FOD data is in close agreement with the global expansion model of eye growth that occurs uniformly with a consequent increase in FOD, our FOC data is consistent with the equatorial stretching model. Thus, our data suggests that while the optic disc shifts nasally as myopia progresses, the outer neural retina does not follow such a stretching pattern.

4.2 High resolution imaging of the peripapillary crescent

As myopia develops, the retina must expand its surface area to cover the increased area of the enlarged eyeball. One of the major clinical signs of retinal stretching is the presence of a peripapillary crescent, which suggests thinning and pulling of the RPE and choroid away from the optic disc. In the present study, the cross sectional configurations of the peripapillary retina were investigated in 6 of the eyes using SDOCT. From the SDOCT images, the incomplete loss of ONL and the absence of the RPE+ layers closely correspond to the extent of the crescents on the infrared fundus images. This structural abnormality within the crescent is also known as peripapillary atrophy. Previous histopathological studies have categorized peripapillary atrophy into zone-α and zone-β. Whereas zone-α shows a disrupted RPE layer, zone-β represents a complete loss of the RPE layer and a partial loss of the photoreceptors at the affected peripapillary retina (Curcio et al., 2000; Fantes & Anderson, 1989; Kubota et al., 1993). Therefore, our SDOCT images further support previous histological findings of zone-β atrophy within the crescent. Our results support the hypothesis that as the eye is growing there is slippage of the major retinal layers as the sclera eye grows. This slippage is most apparent at the optic disc, where the tension established by scleral growth appears to be relieved by a separation of the overlying outer retinal layers and RPE.

Of particular note is that one of the subjects showed a localized peripapillary retinoschisis with the retina splitting into two distinct layers within the crescent (Figure 5b). The presence of columns that bridge between the retinal nerve fiber layer and the INL were also seen across the retinoschisis. These bridging elements are suggested to be Muller cells by a previous OCT study (Carbonelli, Savini, Zanini & Barboni, 2007).

Recent advance in AOSLO imaging now allows us to evaluate the structural consequence of crescent formation at cellular level in living eyes. The dual deformable mirror subsystem can correct the dramatic aberrations near the optic disc and allow high resolution imaging of the crescent area. One interesting finding is that AOSLO imaging showed that the cone photoreceptors presented at the temporal margin within the crescent, although it is not clear if these cone photoreceptors were functioning normally. The congruence of the AOSLO imaging and SDOCT imaging supports the ability of the SDOCT to properly identify the retinal layers in the region of pathology.

5. Conclusions

Our data provide a new insight for analyzing the effect of myopic eye growth patterns on the optic disc and optic disc crescent formation. With increasing AL, the FOD increases, as expected by most eye growth models that include posterior pole growth. However, the FOC data clearly show that, at least in the nasal retina, the outer neural retina does not follow such a stretching pattern.

NIH-PA Author Manuscript

NIH-PA Author Manuscript

NIH-PA Author Manuscript

Acknowledgments

The authors acknowledge Drs. Arthur Bradley and Larry N. Thibos for their helpful discussions. This work was supported by NIH Grants R01-EY14375 and R01-EY04395.

This work was supported by NIH grants R01-EY14375, R01-EY04395, and P30EY019008 to SAB.

References

Bennett AG, Rudnicka AR, Edgar DF. Improvements on Littmann's method of determining the size of retinal features by fundus photography. Graefes Arch Clin Exp Ophthalmol. 1994; 232(6):361–367. [PubMed: 8082844]

Burns SA, Wu S, Delori F, Elsner AE. Direct measurement of human-cone-photoreceptor alignment. J Opt Soc Am A Opt Image Sci Vis. 1995; 12(10):2329–2338. [PubMed: 7500214]

Burns SA, Zhong Z, Qi X, Elsner AE. Multi-wavelength imaging and image quality for a dual deformable adaptive optics SLO. Invest Ophthalmol Vis Sci. 2010; 51 E-Abstract 3454.

Carbonelli M, Savini G, Zanini M, Barboni P. Peripapillary detachment in pathologic myopia: Unusual OCT findings. Clin Ophthalmol. 2007; 1(3):327–329. [PubMed: 19668489]

Chui TY, Song H, Burns SA. Adaptive-optics imaging of human cone photoreceptor distribution. J Opt Soc Am A Opt Image Sci Vis. 2008a; 25(12):3021–3029. [PubMed: 19037393]

Chui TY, Song H, Burns SA. Individual variations in human cone photoreceptor packing density: variations with refractive error. Invest Ophthalmol Vis Sci. 2008b; 49(10):4679–4687. [PubMed: 18552378]

Curcio CA, Saunders PL, Younger PW, Malek G. Peripapillary chorioretinal atrophy: Bruch's membrane changes and photoreceptor loss. Ophthalmology. 2000; 107(2):334–343. [PubMed: 10690836]

Curtin BJ, Karlin DB. Axial length measurements and fundus changes of the myopic eye. Am J Ophthalmol. 1971; 1(1 Part 1):42–53. [PubMed: 5099937]

Fantes FE, Anderson DR. Clinical histologic correlation of human peripapillary anatomy. Ophthalmology. 1989; 96(1):20–25. [PubMed: 2919048]

Ferguson RD, Zhong Z, Hammer DX, Mujat M, Patel AH, Deng C, Zou W, Burns SA. Adaptive optics scanning laser ophthalmoscope with integrated wide-field retinal imaging and tracking. J Opt Soc Am A Opt Image Sci Vis. 2010; 27(11):A265–A277. [PubMed: 21045887]

Fulk GW, Goss DA, Christensen MT, Cline KB, Herrin-Lawson GA. Optic nerve crescents and refractive error. Optom Vis Sci. 1992; 69(3):208–213. [PubMed: 1565418]

Grossniklaus HE, Green WR. Pathologic findings in pathologic myopia. Retina. 1992; 12(2):127–133. [PubMed: 1439243]

Hendicott P, Lam C. Myopic crescent, refractive error and axial length in Chinese eyes. Clin Exp Optom. 1991; 74(5):168–174.

Jonas JB, Nguyen XN, Gusek GC, Naumann GO. Parapapillary chorioretinal atrophy in normal and glaucoma eyes. I. Morphometric data. Invest Ophthalmol Vis Sci. 1989; 30(5):908–918. [PubMed: 2722447]

Kubota T, Jonas JB, Naumann GO. Direct clinico-histological correlation of parapapillary chorioretinal atrophy. Br J Ophthalmol. 1993; 77(2):103–106. [PubMed: 8435408]

Miller DT, Williams DR, Morris GM, Liang J. Images of cone photoreceptors in the living human eye. Vision Res. 1996; 36(8):1067–1079. [PubMed: 8762712]

Mok KH, Lee VW. Disc-to-macula distance to disc-diameter ratio for optic disc size estimation. J Glaucoma. 2002; 11(5):392–395. [PubMed: 12362077]

Nakazawa M, Kurotaki J, Ruike H. Longterm findings in peripapillary crescent formation in eyes with mild or moderate myopia. Acta Ophthalmol. 2008; 86(6):626–629. [PubMed: 18577184]

Rohrschneider K. Determination of the location of the fovea on the fundus. Invest Ophthalmol Vis Sci. 2004; 45(9):3257–3258. [PubMed: 15326148]

Roorda A, Williams DR. Optical fiber properties of individual human cones. J Vis. 2002; 2(5):404–412. [PubMed: 12678654]

NIH-PA Author Manuscript

NIH-PA Author Manuscript

NIH-PA Author Manuscript

Stiles WS, Crawford BH. The luminous efficiency of rays entering the eye pupil at different points. Proc R Soc Lond B. 1933; 112(778):428–450.

Strang NC, Winn B, Bradley A. The role of neural and optical factors in limiting visual resolution in myopia. Vision Res. 1998; 38(11):1713–1721. [PubMed: 9747504]

van Blokland GJ. Directionality and alignment of the foveal receptors, assessed with light scattered from the human fundus in vivo. Vision Res. 1986; 26(3):495–500. [PubMed: 3727414]

Williams TD, Wilkinson JM. Position of the fovea centralis with respect to the optic nerve head. Optom Vis Sci. 1992; 69(5):369–377. [PubMed: 1594198]

Yasuzumi K, Ohno-Matsui K, Yoshida T, Kojima A, Shimada N, Futagami S, Tokoro T, Mochizuki M. Peripapillary crescent enlargement in highly myopic eyes evaluated by fluorescein and indocyanine green angiography. Br J Ophthalmol. 2003; 87(9):1088–1090. [PubMed: 12928272]

NIH-PA Author Manuscript

NIH-PA Author Manuscript

NIH-PA Author Manuscript

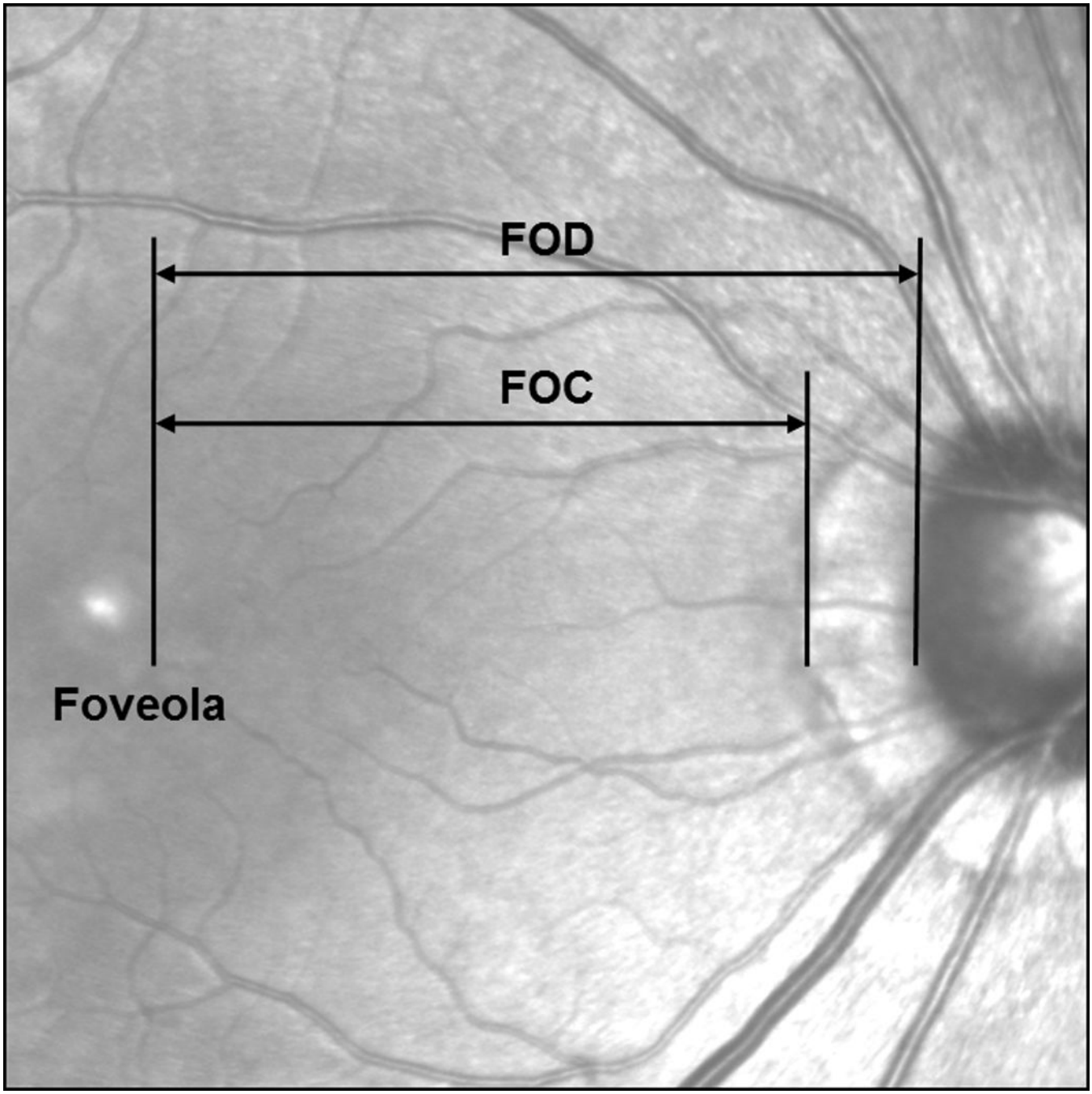

Figure 1.
Retinal distances measured on the infrared fundus image. Both FOD and FOC were measured along the horizontal axis from the foveola to the optic disc margin or the crescent margin.

NIH-PA Author Manuscript

NIH-PA Author Manuscript

NIH-PA Author Manuscript

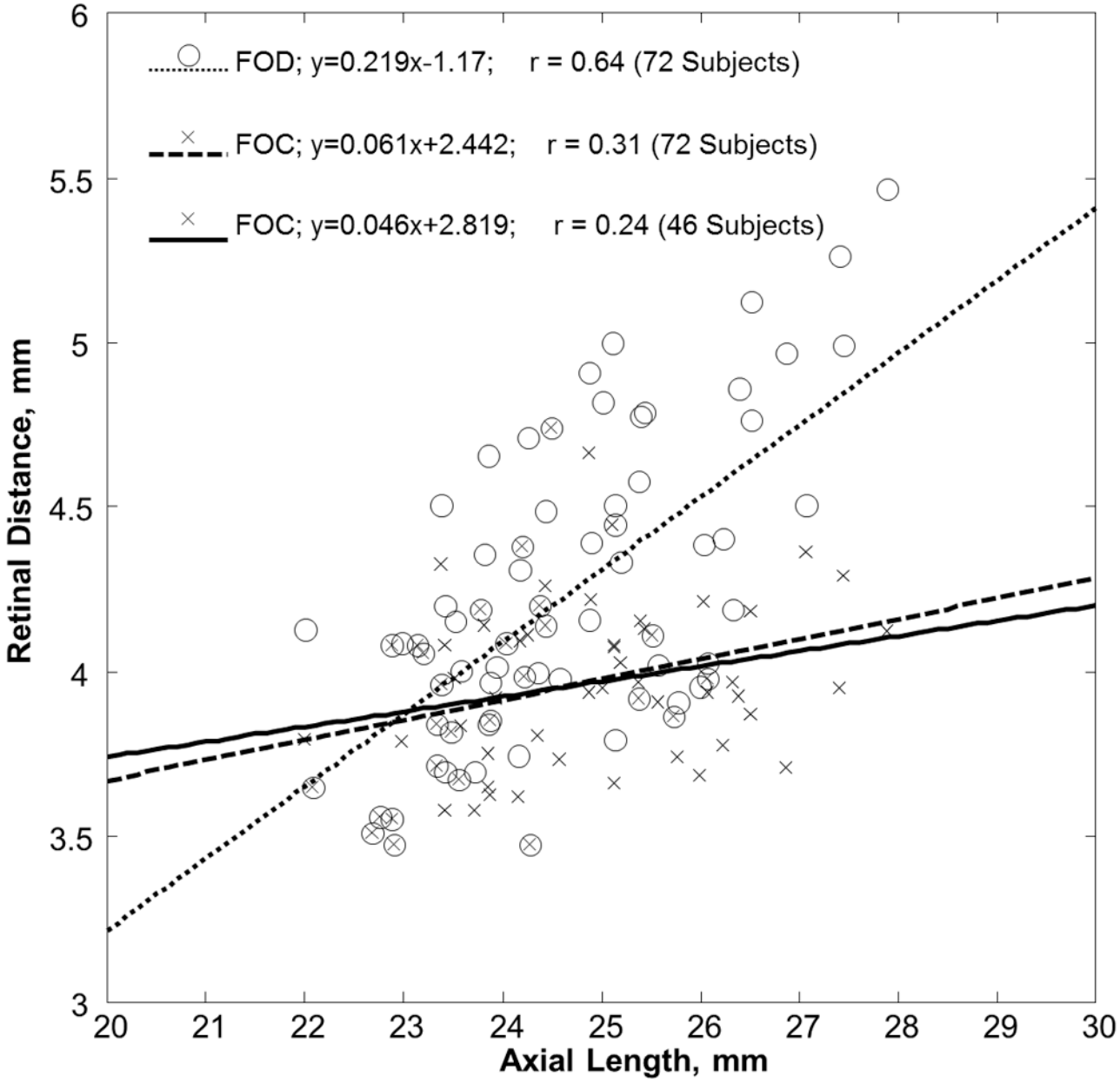

Figure 2.

Variation of retinal distance with axial length. Open symbols represent the retinal distance from the foveola to the temporal edge of the optic disc (FOD). Cross symbols represent the retinal distance from the foveola to the temporal edge of the crescent (FOC). The dotted and dashed lines represent the linear regression fit of the FOD and FOC in 72 subjects, respectively. The solid line represents the linear regression fit of the FOC in 46 subjects who had optic disc crescent.

NIH-PA Author Manuscript
NIH-PA Author Manuscript
NIH-PA Author Manuscript

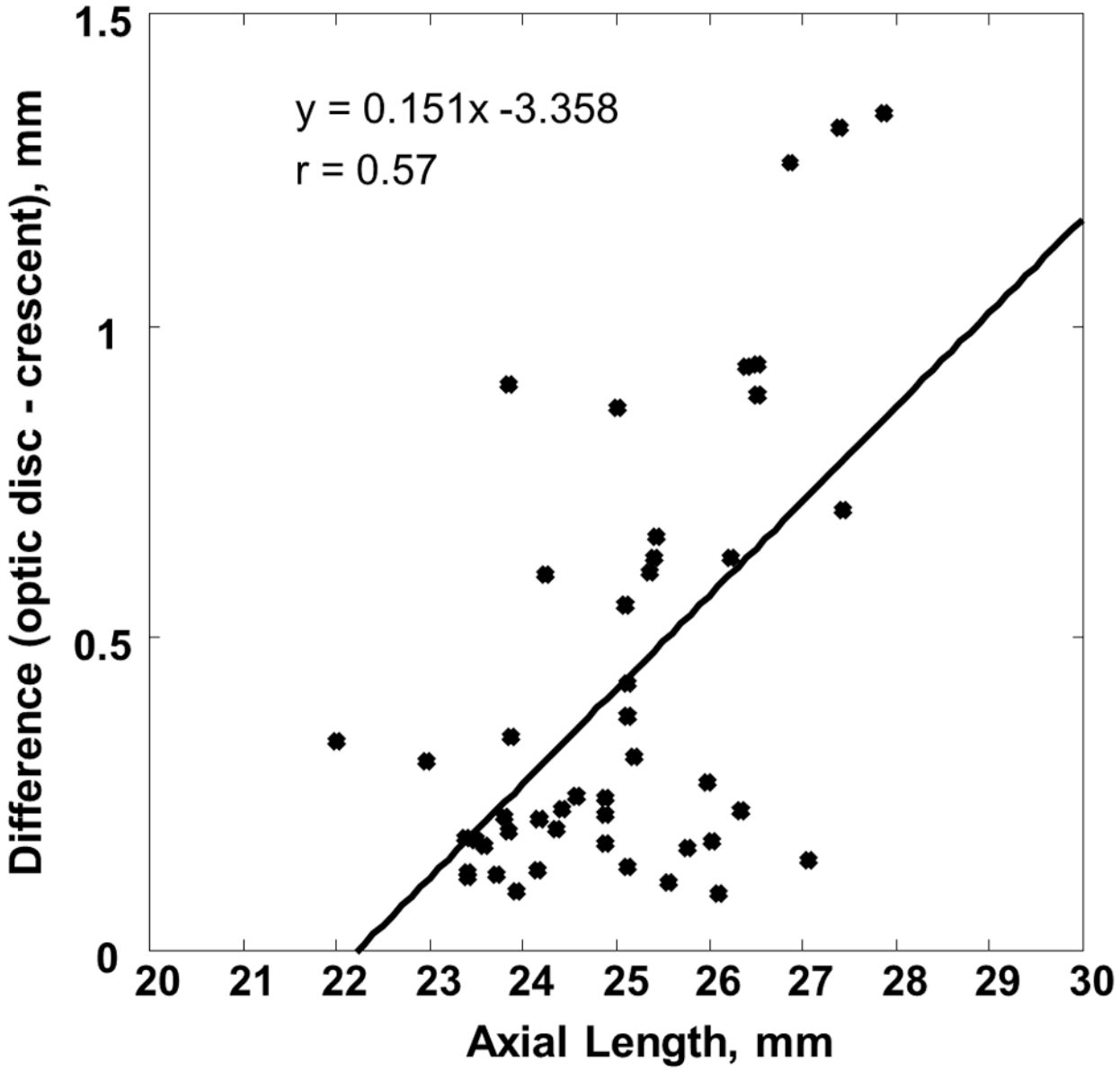

Figure 3.
The difference of FOD and FOC as a function of axial length. Optic disc crescent presents in 64% of the subjects with an average of 0.42mm in width. Linear regression to the data is showed by the solid line.

NIH-PA Author Manuscript

NIH-PA Author Manuscript

NIH-PA Author Manuscript

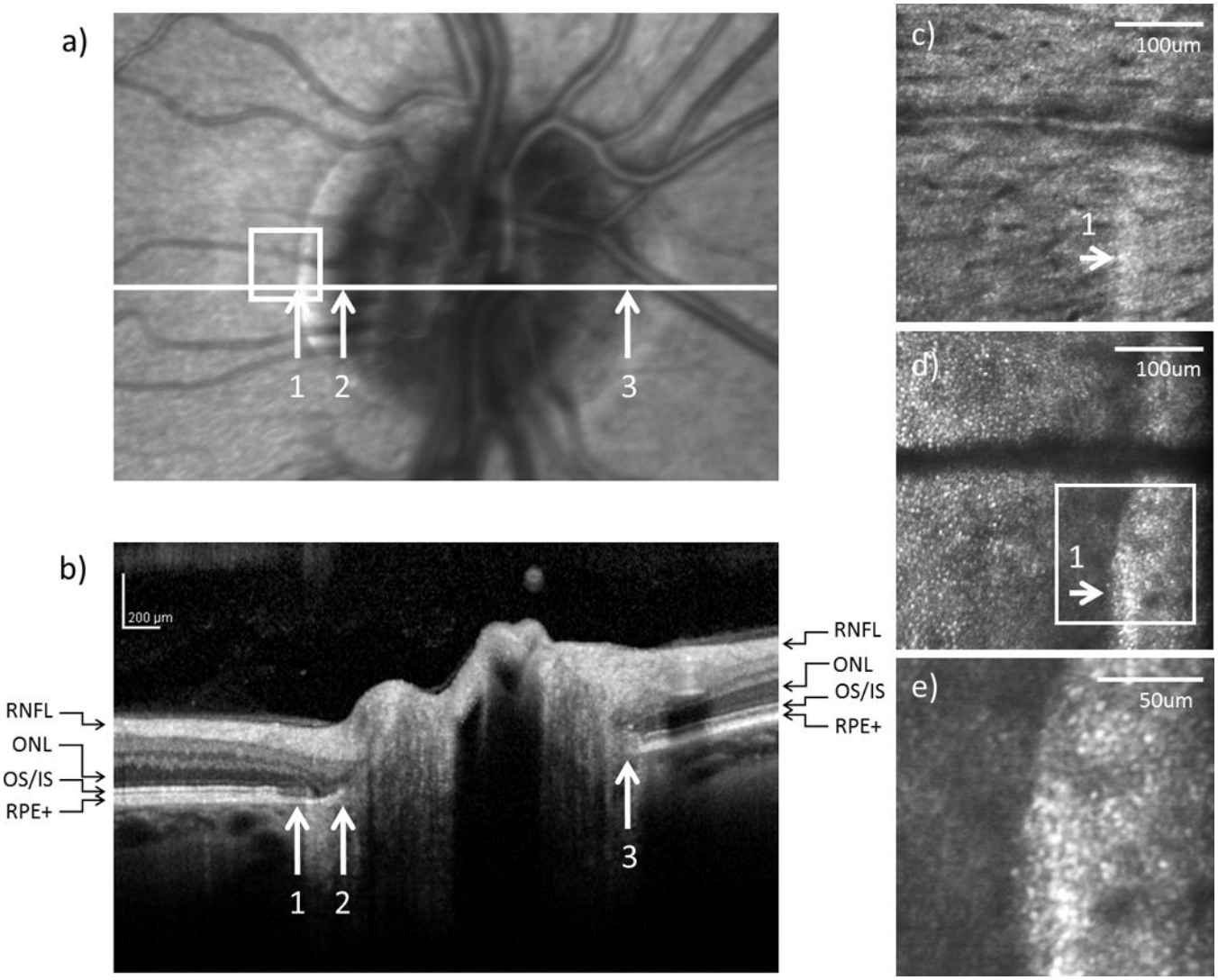

Figure 4.

(a) Infrared and (b) SDOCT images of the optic disc in subject 1. Arrows indicate (1) the temporal edge of the crescent, (2) the temporal edge of the optic disc, and (3) the nasal edge of the optic disc. The SDOCT scan across the optic disc as indicated by the white horizontal line in (a) is shown in (b) (RNFL = retinal nerve fiber layer; ONL = outer nuclear layer; OS/IS = junction of outer segment and outer segment of photoreceptors; RPE+ = retinal pigment epithelium complex). High resolution AOSLO images of (c) RNFL and (d) cone photoreceptor on the temporal edge of the crescent as indicated by the white box on (a), arrows indicate the edge of the crescent. (e) Magnified view of the crescent as indicated by the white box on (d).

NIH-PA Author Manuscript

NIH-PA Author Manuscript

NIH-PA Author Manuscript

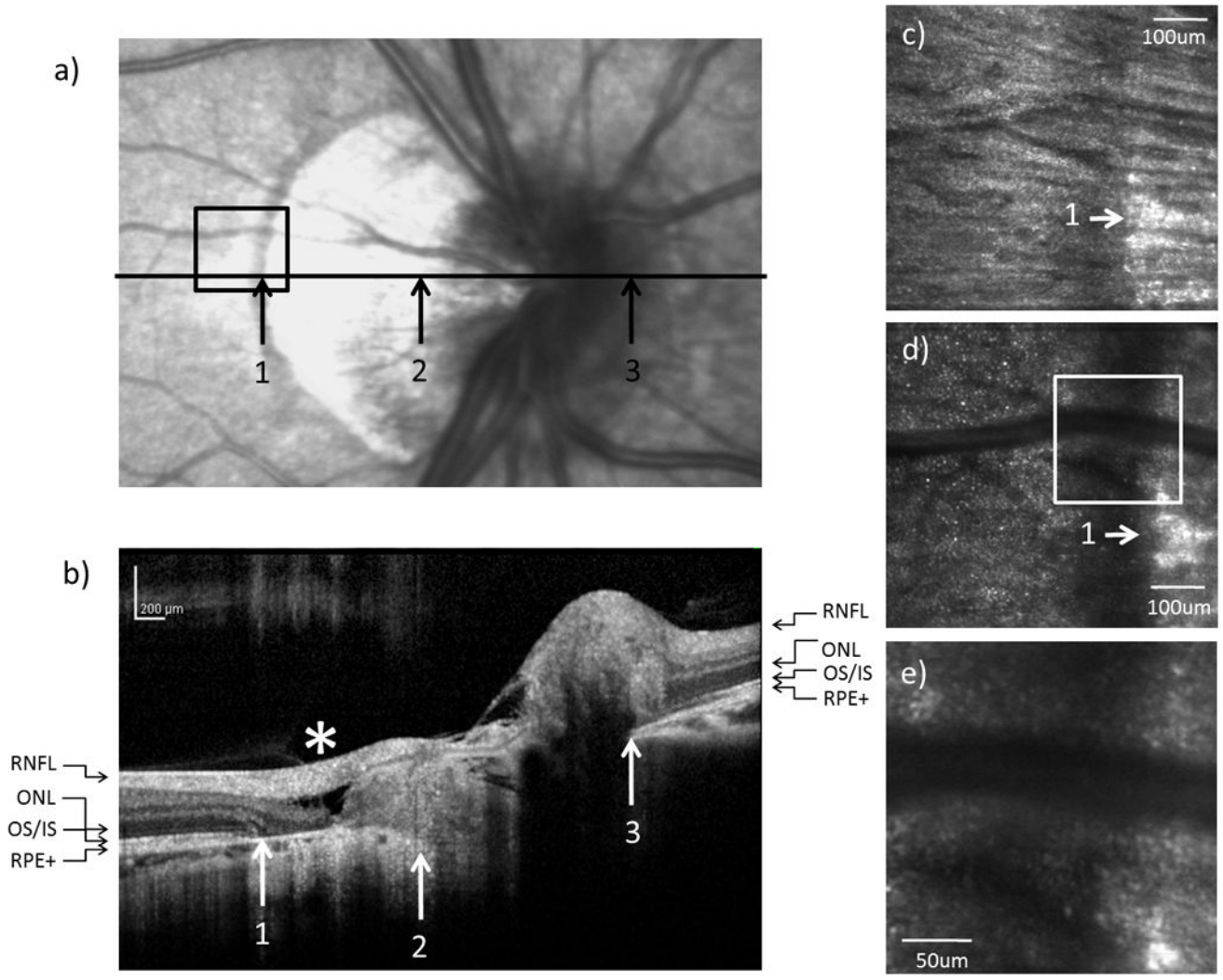

Figure 5.

(a) Infrared and (b) SDOCT images of the optic disc in subject 3. High resolution AOSLO images of (c) RNFL and (d) cone photoreceptor on the temporal edge of the crescent as indicated by the black box on (a). (e) Magnified view of the crescent as indicated by the white box on (d). * indicates retinal slippage.

NIH-PA Author Manuscript

NIH-PA Author Manuscript

NIH-PA Author Manuscript

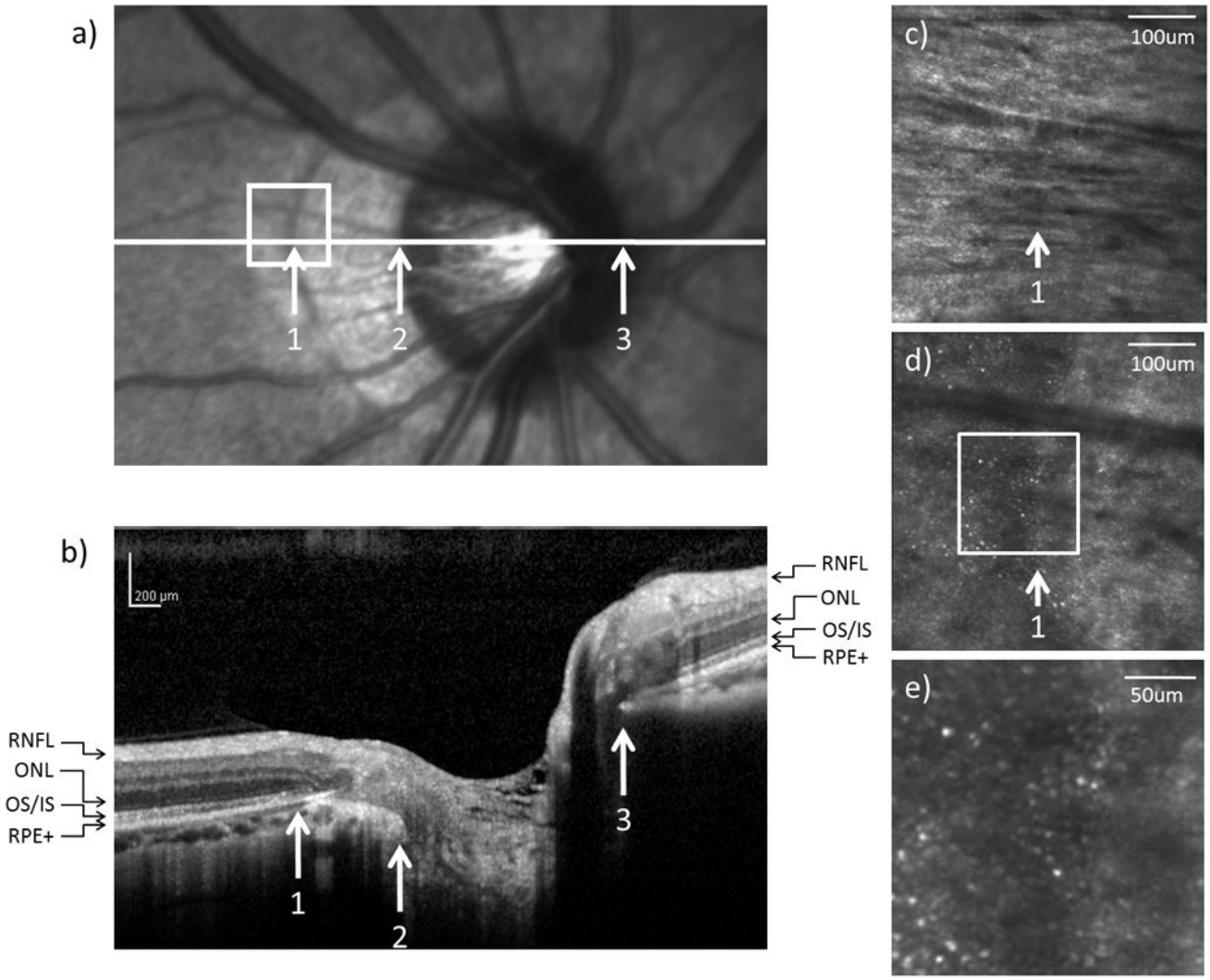

Figure 6.
(a) Infrared and (b) SDOCT images of the optic disc in subject 5. High resolution AOSLO images of (c) RNFL and (d) cone photoreceptor on the temporal edge of the crescent as indicated by the white box on (a). (e) Magnified view of the crescent as indicated by the white box on (d).

NIH-PA Author Manuscript

NIH-PA Author Manuscript

NIH-PA Author Manuscript

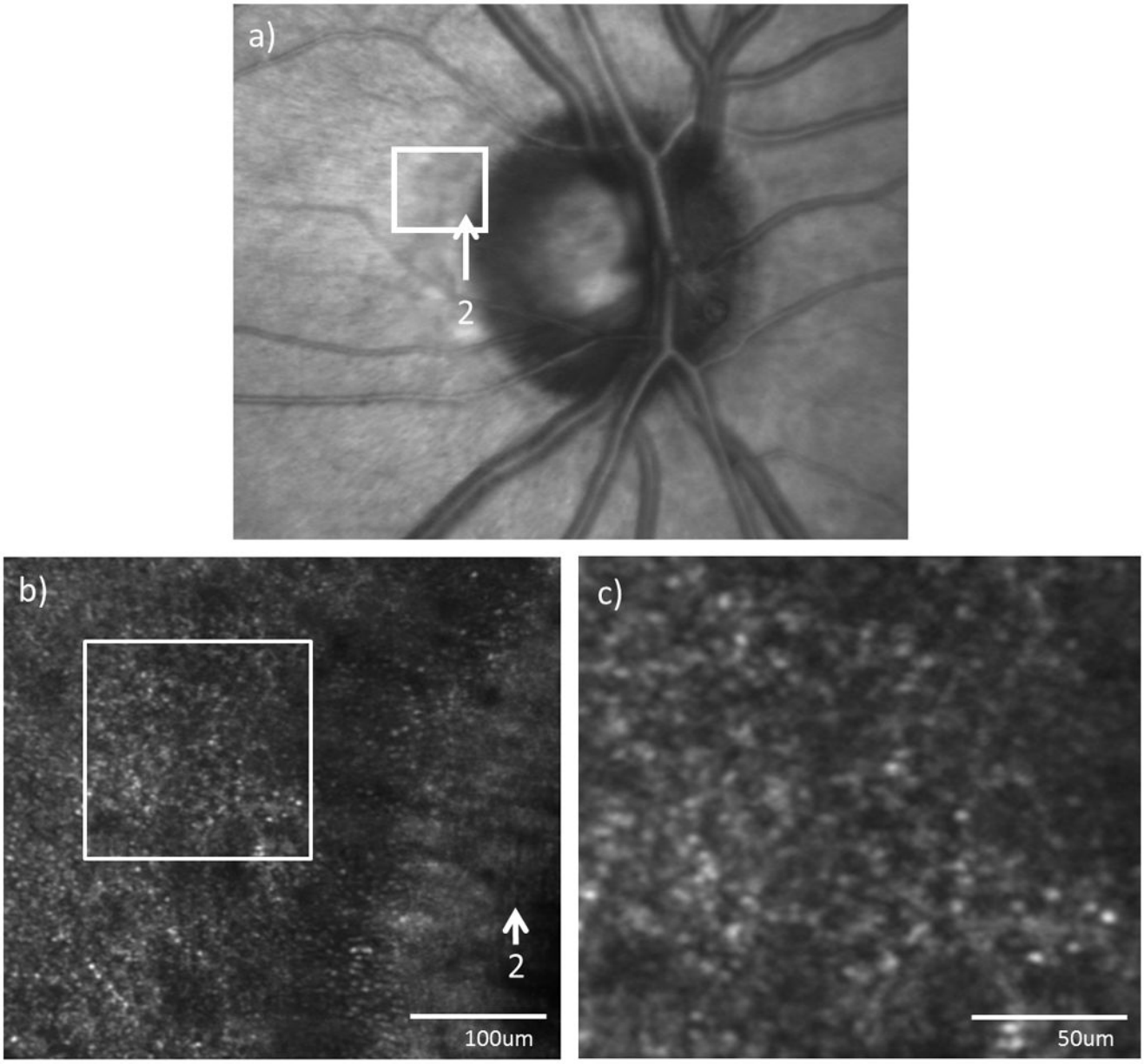

Figure 7.
(a) Infrared fundus image and (b) high resolution AOSLO images of the optic disc edge in subject 4. Arrows indicate the temporal edge of the optic disc. (c) Magnified view of the AOSLO image as indicated by the white box on (b).

NIH-PA Author Manuscript
NIH-PA Author Manuscript
NIH-PA Author Manuscript

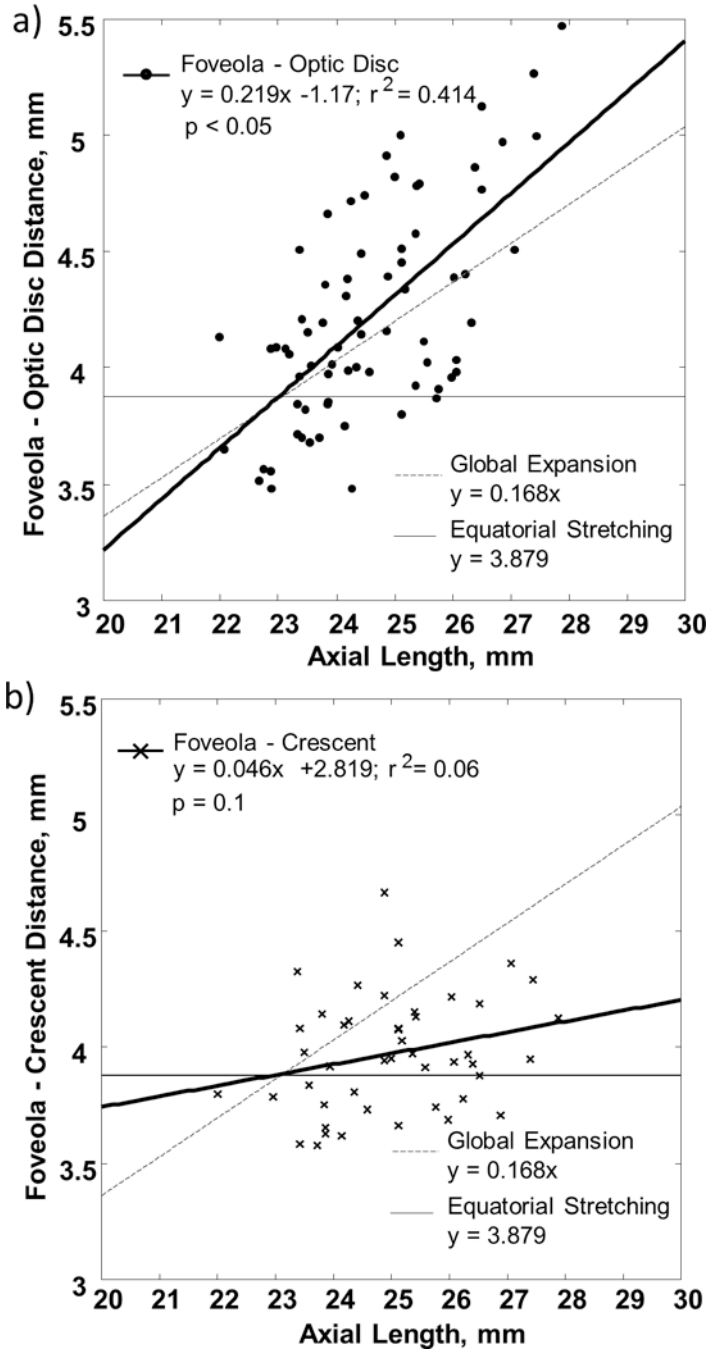

Figure 8.

a) FOD and b) FOC as a function of axial length. Linear regressions to the data are showed by the heavy solid lines. The light solid lines indicate the prediction of FOD and FOC by the equatorial stretching model. The dashed lines indicate the prediction of FOD and FOC by the global expansion model.

NIH-PA Author Manuscript

NIH-PA Author Manuscript

NIH-PA Author Manuscript

Table 1

Demographic data of the 6 subjects tested with SDOCT and AOSLO.

Subject no.	Age	Rx (D)	AL (mm)	Crescent width (mm)
1 (AB)	54	+0.50	23.50	0.175
2 (SJ)	31	−6.75	25.42	0.662
3 (RL)	24	−8.25	26.87	1.263
4 (ZZ)	24	−6.00	25.51	0
5 (GH)	26	−4.75	26.51	0.891
6 (XQ)	43	−4.75	26.23	0.629
mean±SD	33.67±12.27	−5.00±3.00	25.67±1.20	0.60±0.46